ZEUS-prel-06-008

Submitted to the
XXIII International Conference on High Energy Physics
July 26-August 2, Moscow, Russia

Session: QCD soft interactions

Heavy-stable particle production in neutral current deep inelastic scattering at HERA

Abstract

The production of antideuterons and (anti)protons was studied in deep inelastic ep scattering with the ZEUS detector at HERA. The data sample consists of deep inelastic ep scattering events at a centre-of-mass energy of 300–318 GeV and $Q^2 > 1\,\mathrm{GeV}^2$, and corresponds to 120 pb^{-1} integrated luminosity. No antitritons were found. The antideuteron production rate is three to four orders of magnitude smaller than the antiproton yield, which is in agreement with other measurements.

1 Introduction

Light-stable nuclei, such as deuterons (d) and tritons (t), are loosely bound states whose production in high energy collisions can hardly be accommodated in the standard hadronisation models. In collisions involving elementary particles, the underlying production mechanism of such states is poorly understood. The production rate of antideuterons in $e^+e^- \rightarrow q\bar{q}$ collisions [1, 2, 3] is significantly lower than that measured in hadronic $\Upsilon(1S)$ and $\Upsilon(2S)$ decays [1]. The antideuteron rate in $e^+e^- \rightarrow q\bar{q}$ is also lower than that in hadronic (pA [4,5], pp [6]) and photonic collisions with protons (γp) at HERA [7], but higher than that in nucleus-nucleus (AA) collisions [8, 9]. Usually, the coalescence model [10] is used to explain the production of the heavy-stable charged particles. According to this model, the production rate is determined by the overlap between the wave function of a proton and a neutron with the wave function of a deuteron.

At present, neither $\bar{d}$ nor $\bar{t}$ has been reported in deep inelastic scattering (DIS). This paper presents the results of a search for heavy-stable charged particles in the central rapidity region of ep collisions at HERA. The analysis was performed using DIS events which are characterised by the presence of a scattered lepton. Such events provide an ideal environment in which the background contribution from non-ep interactions is minimal.

2 Experimental set-up

A detailed description of the ZEUS detector can be found elsewhere [11]. A brief outline of the components that are most relevant for this analysis is given below.

Charged particles are tracked in the central tracking detector (CTD) [12], which operates in a magnetic field of 1.43 T provided by a thin superconducting solenoid. The CTD consists of 72 cylindrical drift chamber layers, organized in nine superlayers covering the polar-angle[1] region $15^\circ < \theta < 164^\circ$. The transverse-momentum resolution for full-length tracks is $\sigma(p_T)/p_T = 0.0058 p_T \oplus 0.0065 \oplus 0.0014/p_T$, with p_T in GeV. To estimate the ionization energy loss per unit length, dE/dx, of particles in the CTD [13], the truncated mean of the anode-wire pulse heights was calculated, which removes the lowest 10% and at least the highest 30% depending on the number of saturated hits. The measured dE/dx values were corrected by normalising to the average dE/dx for tracks around the region of minimum ionisation for pions, $0.3 < p < 0.4$ GeV. Henceforth, dE/dx is quoted in

[1] The ZEUS coordinate system is a right-handed Cartesian system, with the Z axis pointing in the proton beam direction, referred to as the "forward direction", and the X axis pointing left towards the centre of HERA. The coordinate origin is at the nominal interaction point.

units of minimum ionising particles (mips). The resolution of the dE/dx measurement for full-length tracks is about 9%.

The high-resolution uranium–scintillator calorimeter (CAL) [14] consists of three parts: the forward, the barrel and the rear calorimeters. Each part is subdivided transversely into towers and longitudinally into one electromagnetic section and either one or two hadronic sections. The smallest subdivision of the calorimeter is called a cell. The CAL energy resolutions, as measured under test-beam conditions, are $\sigma(E)/E = 0.18/\sqrt{E}$ for electrons and $\sigma(E)/E = 0.35/\sqrt{E}$ for hadrons, with E in GeV. A presampler [15] mounted in front of the calorimeter was used to correct the energy of the scattered electron[2]. The position of electrons scattered close to the electron beam direction is determined by a scintillator-strip detector [16].

The luminosity was measured using the bremsstrahlung process $ep \rightarrow ep\gamma$ with the luminosity monitor [17], a lead–scintillator calorimeter placed in the HERA tunnel at $Z = -107$ m.

3 Event sample

The data sample, collected with the ZEUS detector at HERA, corresponds to an integrated luminosity of 120 pb^{-1}, taken between 1996 and 2000. This sample is the sum of 39 pb^{-1} of e^+p data taken at a centre-of-mass energy of 300 GeV and 64 pb^{-1} taken at 318 GeV, plus 17 pb^{-1} of e^-p data taken at 318 GeV.

The search was performed using DIS events with exchanged-photon virtuality $Q^2 \geq 1\,\text{GeV}^2$ as in a previous ZEUS publication [18]. The Bjorken scaling variables x and y, as well as Q^2, were reconstructed using the electron method (denoted by the subscript e), which uses measurements of the energy and angle of the scattered electron, or using the Jacquet-Blondel (JB) method [19]. The scattered-electron candidate was identified from the pattern of energy deposits in the CAL [20].

The following requirements were imposed:

- $Q^2_e \geq 1\,\text{GeV}^2$;
- the impact point of the scattered electron on the RCAL outside the (X, Y) region (24cm, 12cm) centered on the beamline;
- $E_{e'} \geq 8.5\,\text{GeV}$, where $E_{e'}$ is the corrected energy of the scattered electron measured in the CAL;

[2] Henceforth the term electron is used to refer both to electrons and positrons.

- $35 \leq \delta \leq 65$ GeV, where $\delta = \sum E_i(1 - \cos\theta_i)$, E_i is the energy of the ith calorimeter cell, θ_i is its polar angle and the sum runs over all cells;
- $y_e \leq 0.95$ and $y_{\mathrm{JB}} \geq 0.01$;
- $\mid Z_{\mathrm{vertex}} \mid \leq 40\,\mathrm{cm}$ and $\sqrt{X^2_{\mathrm{vertex}} + Y^2_{\mathrm{vertex}}} \leq 1\,\mathrm{cm}$, where Z_{vertex}, X_{vertex} and Y_{vertex} are the coordinates of the vertex position determined from the tracks;
- events were accepted with at least three tracks fitted to the primary vertex. This cut was used to reduce the background from beam-gas events and to insure a good reconstruction of the primary vertex.

The CTD tracks were required to have at least 40 CTD hits and transverse momenta $p_T \geq 0.15\,\mathrm{GeV}$, restricting the study to a region where the CTD track acceptance and resolution are high.

For each track, the following additional variables are reconstructed:

- the distance, ΔZ, of the Z-component of the track helix to the primary vertex given by Z_{vertex};
- the distance of closest approach (DCA) of the track to the beam spot in the transverse plane. The beam-spot positions in x and y were reconstructed from the average primary-vertex distribution for each data taking period.

The (anti)proton and (anti)deuteron selection used the energy-loss measurement in the CTD, dE/dx. To ensure a good dE/dx measurement, only tracks with more than 8 samplings for the dE/dx measurement after truncation [21] were used.

Figure 1 shows the dE/dx distribution as a function of the track momentum for positive and negative tracks. The events were selected by requiring at least one track with $dE/dx >$ 2.5 mips. To reduce the fraction of tracks coming from non-ep collisions, tracks are required to have $|\Delta Z| < 1\,\mathrm{cm}$ and $|DCA| < 0.5\,\mathrm{cm}$. After such a selection, clear bands corresponding to charged kaons, protons and deuterons are observed. The requirement $dE/dx > 2.5$ mips enhances the fraction of events with at least one particle with a mass larger than the pion mass and leads to the discontinuity near $dE/dx = 2.5$ mips seen in Figure 1. The lines show the mean dE/dx from the expectations based on the Bethe-Bloch equation.

Figure 2 shows the reconstructed masses, M, for different particle species. The mass was calculated from the measured track momentum and energy loss using an analytical parametrisation of the most probable energy loss. The Gaussian peaks for negative and positive tracks are shifted, since CTD response for negative and positive tracks is expected to be different. The number of deuterons and antideuterons in the mass window $1.5 < M < 2.5\,\mathrm{GeV}$ is 309 and 62, respectively.

No antitritons were observed. Given the small number of triton candidates, no conclusive statement on the observation of t states in DIS can be made.

Figure 3 shows a typical DIS event with an antideuteron. This event, found using the mass cut $1.5 < M < 2.5\,\text{GeV}$, has the following characteristics: $Q_e^2 = 45.5\,\text{GeV}^2$, $E_{e'} = 14.3\,\text{GeV}$, 12 tracks fitted to the primary vertex, and $Z_{\text{vertex}} = -5.4\,\text{cm}$. The antideuteron candidate, indicated by an arrow, has $dE/dx = 2.7$ mips and the momentum $p = 1.1\,\text{GeV}$. The BCAL energy corresponding to this antideuteron is 3.2 GeV.

4 Monte Carlo samples

For the checks done in this paper, the ARIADNE Monte Carlo (MC) model [22] for the description of fully inclusive DIS events was used. The MC sample corresponds to an integrated luminosity of $75\,\text{pb}^{-1}$. This MC does not include a mechanism for the production of (anti)deuteron and (anti)tritons. The generated events were passed through a full simulation of the detector using GEANT 3.13 [23], after which a clear dE/dx band for deuterons produced by secondary interactions with the detector material was observed. However, no antideuteron signal appears in the MC sample.

For studies of reconstruction efficiencies, a second MC sample was generated after the inclusion of deuterons at the generator level. Deuterons were included in the MC sample by combining protons and neutrons with similar momenta at the generator level. Then the generated events were passed through a full simulation of the detector.

5 Identification of particles produced in *ep* collisions

The identification of heavy-stable charged particles requires studies of several sources of background processes:

- events due to interactions of the proton (or electron) beam with residual gas in the beam pipe (termed beam-gas interactions);
- secondary interactions of particles on inactive material between the interaction point and the central tracking detector.

Both background contributions for particles produced in *ep* collisions will be discussed below.

5.1 Beam-gas interactions

The contribution from beam-gas interactions is significantly reduced after the ZEUS three-level trigger which requires a scattered lepton in the CAL. In addition, the requirement to accept only events with more than three tracks fitted to the primary vertex significantly reduces the contribution from beam-gas events. The remaining fraction of the beam-gas interactions can be assessed by studying the Z_{vertex} distribution and DIS-related kinematic variables (both will be discussed below). The Z_{vertex} distributions for events with at least one (anti)proton or (anti)deuteron candidate were reconstructed using the mass cuts $0.7(0.6) < M < 1.5\,\mathrm{GeV}$ and $1.5 < M < 2.5\,\mathrm{GeV}$ respectively. Due to a shift in the dE/dx for negative tracks, the lower mass cut for antiprotons was at 0.6 GeV. In addition, it is required $|\Delta Z| < 2(1)\,\mathrm{cm}$ and $|DCA| < 1.5(0.5)\,\mathrm{cm}$ for p (d) candidates. These cuts are less tight for protons since the proton ΔZ and DCA distributions were found to be wider than those for the heavy states (see Sect. 5.2).

Figure 4 shows the Z_{vertex} distribution for (anti)protons and (anti)deuterons. The data distributions were fitted using a Gaussian function with a first-order polynomial for the background description. The extracted Gaussian widths are fully consistent with those obtained for fully-inclusive DIS events without the deuteron preselection. Figure 4 shows that there is essentially no beam-gas background for antideuteron events. A small background for deuterons at positive Z_{vertex} is mainly due to secondary interactions, since the MC distribution generated for fully inclusive DIS events showed a similar contamination. However, beam-gas events are also expected to contribute at $\mid Z_{\mathrm{vertex}} \mid > 40\,\mathrm{cm}$. If one assumes that the background seen in Fig. 4(c) is due to proton-gas or electron-gas events, then the contribution from the beam-gas interactions does not exceed 20% of the total number of events with deuterons.

5.2 Secondary interactions on inactive material

Even for a clean DIS sample, deuterons can still be produced by secondary interactions of particles on inactive material. The requirement to accept only primary tracks, i.e. tracks which point to the primary vertex, reduces efficiently such contributions, removing all tracks which have $|DCA|$ larger than 0.5–1.0 cm. However, this method was not used since, in this case, it is difficult to estimate the fraction of secondary-scattering tracks in the region of small $|DCA|$. Therefore, the extraction of deuteron candidates was performed using the DCA distribution after the cut on the ΔZ distribution, $\mid \Delta Z \mid < 2(1)\,\mathrm{cm}$ for p (d) (see Fig. 5). The DCA distributions, shown in Fig. 6, were reconstructed from all the tracks after the cuts described in Sect. 3. After the cut on the ΔZ distribution and the mass cuts, clear peaks are observed for proton and deuteron candidates. The number of particles associated with the primary ep vertex was assessed by using the side-band background subtraction. For this procedure, a linear fit to the events on either side of the peak region in the range $2 <| DCA |< 5$ cm was performed and the average value was subtracted. The signal region was $| DCA |< 1.5(0.5)$ cm for p (d) candidates.

The number of reconstructed (anti)protons in the data after the DCA side-band background subtraction was 1.61×10^5 (1.74×10^5). The proton-antiproton asymmetry is mainly due to different dE/dx efficiencies and the mass cuts shown in Fig. 2 for positive and negative tracks. The number of deuterons and antideuterons, after the side-band background subtraction, is 195 ± 18 and 61 ± 8, respectively. Such a large difference cannot be explained by the charge asymmetry in the selection efficiency but may be due to the presence of a residual background from secondary interactions peaking at small DCA in the deuteron sample. Since this observation requires further studies, the $d/\bar{d}$ and d/p ratios corrected for detector effects are not given in this paper.

Figure 7 shows the distributions for several DIS kinematic variables: Q^2_e, x, $E_{e'}$ and δ. The numbers of antideuteron and antiproton candidates were calculated in each bin from the DCA distributions after the side-band background subtraction. The shapes of antideuteron $E_{e'}$ and δ distributions show some deviations with respect to the corresponding antiproton distributions, but still are compatible within statistical uncertainties.

6 Detector corrections and systematical checks

For comparisons with other experiments, the (anti)proton rate was corrected for by removing the decay products of Λ, since most experiments use the coalescence model in which the (anti)deuterons can only be produced directly. The correction factor, estimated from a MC simulation, was 0.793.

The detector correction closely follows the method discussed in [7]. In this approach, efficiency corrections, ε, due to the track reconstruction were estimated separately for protons and deuterons using the ARIADNE MC model (with deuterons included at the generator level). The efficiencies, calculated separately for p, $\bar{p}$ and d, were close to 0.96 for the p_T range used in this analysis, with $\varepsilon(\bar{p})/\varepsilon(p) = 0.95$. For antideuterons, the efficiency correction was estimated as $\varepsilon(\bar{d}) = \varepsilon(d)\varepsilon(\bar{p})/\varepsilon(p)$ for the same p_T range of $p(\bar{p})$ and d.

The inefficiency due to track migrations across the dE/dx cut was estimated using $\Lambda \to p\pi$ decays. In this approach, protons were identified from the Λ peak and then the proton dE/dx selection efficiency was reconstructed as the ratio of the events without and with the dE/dx requirement.

The following systematical uncertainties were considered:

- variations of the DIS-selection cuts. The cut on the energy of the scattered electron was increased to 10 GeV, and the lower cut on the δ distribution was tightened to 40 GeV. The cut on Z_{vertex} was varied by ± 5 cm. The cut on the number of primary tracks was increased from three to four. Variations of the event-selection cuts on y_e and y_{JB} distributions showed a small effect;
- variations in the particle yields associated with the signal extraction: (a) The number of (anti)deuterons were reconstructed using a Gaussian fit of the DCA with a first-order polynomial for the background description. (b) For the side-band background subtraction, the region used to determine the background was reduced to $1.5 <\mid DCA \mid< 3.5$ cm. (c) The DCA cut for the side-band background subtraction was varied within its resolution of ± 0.1 cm. (d) In addition, for the side-band background subtraction, the background shape was taken from the MC (without deuterons at the generator level).
- the cut on ΔZ was varied by 0.2 cm;
- the correction for Λ decays was changed by $\pm 10\%$ (this affects only the d/p and $\bar{d}/\bar{p}$ ratios);
- the inefficiency correction for antideuterons was varied by $\pm(1 - \varepsilon(\bar{p})/\varepsilon(p))$.

The overall systematic uncertainty was determined by adding the above uncertainties in quadrature. The largest experimental uncertainty comes from the signal extraction and the correction procedure.

7 Results and conclusions

The detector-corrected $\bar{d}/\bar{p}$ ratio as a function of p_T/M is shown in Fig. 8. There is a good agreement with the H1 published data for photoproduction [7], as well as with pp data [6]. A similar ratio was also observed in hadronic $\Upsilon(1S)$ and $\Upsilon(2S)$ decays by the ARGUS Collaboration [1].

The $\bar{p}/p$ ratio as a function of p_T/M is shown in Fig. 8(bottom plot). For the given statistics, the $\bar{p}/p$ ratio is consistent with unity.

The events containing at least one antideuteron were analysed in the Breit frame [24]. The number of events with antiprotons in the current region of the Breit frame was less than 1% of the total number of observed events with antiprotons. In this region, no $\bar{d}$ was found. Since the current region of the Breit frame is analogous to a single hemisphere of

e^+e^-, the observation of antideuterons reported in this paper is not in contradiction with the small antideuteron rate observed in $e^+e^- \to q\bar{q}$ [1, 2, 3].

In conclusion, a first observation of antideuterons in ep collisions in the DIS regime at HERA is presented. No antitritons were observed. The production rate of antideuterons is about three to four orders of magnitude smaller than that for antiprotons, which is in broad agreement with other experiments.

Acknowledgements

We thank the DESY Directorate for their strong support and encouragement. The remarkable achievements of the HERA machine group were essential for the successful completion of this work and are greatly appreciated. We are grateful for the support of the DESY computing and network services. The design, construction and installation of the ZEUS detector have been made possible owing to the ingenuity and effort of many people from DESY and home institutes who are not listed as authors. We thank Prof. D. Heinz and Prof. T. Sloan for the discussion of this topic.

References

[1] ARGUS Coll., H. Albrecht et al., Phys. Lett. **B 157**, 326 (1985); ARGUS Coll., H. Albrecht et al., Phys. Lett. **B 236**, 102 (1990).

[2] OPAL Coll., R. Akers, et al.., Z. Phys. **C 67**, 203 (1995).

[3] ALEPH Coll., S. Schael et al. (2006).

[4] IHEP-CERN Coll., F. Binon et al., Phys. Lett. **B 30**, 510 (1969); Yu.M. Antipov et al., Phys. Lett. **B 34**, 164 (1971).

[5] J.W. Cronin et al., Phys. Rev. **D 11**, 3105 (1975).

[6] B. Alper et al., Phys. Lett. **B 46**, 265 (1973); British-Scandinavian Coll., W.M. Gibson et al., Nuovo Cim. Lett. **21**, 189 (1978); V.V. Abramov, Sov. J. Nucl. Phys. **45**, 845 (1987).

[7] H1 Coll., A. Aktas et al., Eur. Phys. J. **C 36**, 413 (2004).

[8] M. Aoki et al., Phys. Rev. Lett. **69**, 2345 (1992); NA52 (NEWMASS) Coll.., G. Appelquist et al., Phys. Lett. **B 376**, 245 (1996); STAR Coll. C. Alper et al., Phys. Rev. Lett. **87**, 262301 (2001); E802 Coll., L. Ahle et al., Phys. Rev. **C 57**, 1416 (1998); NA44 Coll., I.G. Bearden et al., Nucl. Phys. **A 661**, 387 (1999); I.G. Bearden et al., Eur. Phys. J. **C 23**, 237 (2002).

[9] PHENIX Coll., S. S. Adler et al., Phys. Rev. Lett. **94**, 122302 (2005).

[10] S.T. Butler and C.A. Pearson, Phys. Rev. **129**, 836 (1963).

[11] ZEUS Coll., U. Holm (ed.), *The ZEUS Detector*. Status Report (unpublished), DESY (1993), available on `http://www-zeus.desy.de/bluebook/bluebook.html`.

[12] N. Harnew et al., Nucl. Inst. Meth. **A 279**, 290 (1989); B. Foster et al., Nucl. Phys. Proc. Suppl. **B 32**, 181 (1993); B. Foster et al., Nucl. Inst. Meth. **A 338**, 254 (1994).

[13] ZEUS Coll., J. Breitweg et al., Phys. Lett. **B 481**, 213 (2000); ZEUS Coll., J. Breitweg et al., Eur. Phys. J. **C 18**, 625 (2001).

[14] M. Derrick et al., Nucl. Inst. Meth. **A 309**, 77 (1991); A. Andresen et al., Nucl. Inst. Meth. **A 309**, 101 (1991); A. Caldwell et al., Nucl. Inst. Meth. **A 321**, 356 (1992); A. Bernstein et al., Nucl. Inst. Meth. **A 336**, 23 (1993).

[15] A. Bamberger et al., Nucl. Inst. Meth. **A 382**, 419 (1996); S. Magill and S. Chekanov, *Proceedings of the IX Int. Conference on Calorimenry*

(Annecy, Oct 9-14, 2000), B. Aubert et al. (ed.), p. 625. Frascati Physics Series 21, Annecy, France (2001).

[16] A. Bamberger et al., Nucl. Inst. Meth. **A 401**, 63 (1997).

[17] J. Andruszków et al., Preprint DESY-92-066, DESY, 1992;
ZEUS Coll., M. Derrick et al., Z. Phys. **C 63**, 391 (1994);
J. Andruszków et al., Acta Phys. Pol. **B 32**, 2025 (2001).

[18] ZEUS Coll., S. Chekanov et al., Phys. Lett. **B 591**, 7 (2004).

[19] F. Jacquet and A. Blondel, *Proceedings of the Study for an ep Facility for Europe*, U. Amaldi (ed.), p. 391. Hamburg, Germany (1979). Also in preprint DESY 79/48.

[20] H. Abramowicz, A. Caldwell and R. Sinkus, Nucl. Inst. Meth. **A 365**, 508 (1995).

[21] O. Deppe, *Measurement of $D^{\star\pm}$ Electroproduction at HERA*. Ph.D. Thesis, Hamburg University, Hamburg (Germany), Report DESY-THESIS-2000-006, 1999.

[22] L. Lönnblad, Comp. Phys. Comm. **71**, 15 (1992).

[23] R. Brun et al., GEANT3, Technical Report CERN-DD/EE/84-1, CERN, 1987.

[24] R.P. Feynman, *Photon-Hadron Interactions*. Benjamin, New York, 1972;
K.H. Streng, T.F. Walsh and P.M. Zerwas, Z. Phys. **C 2**, 237 (1979).

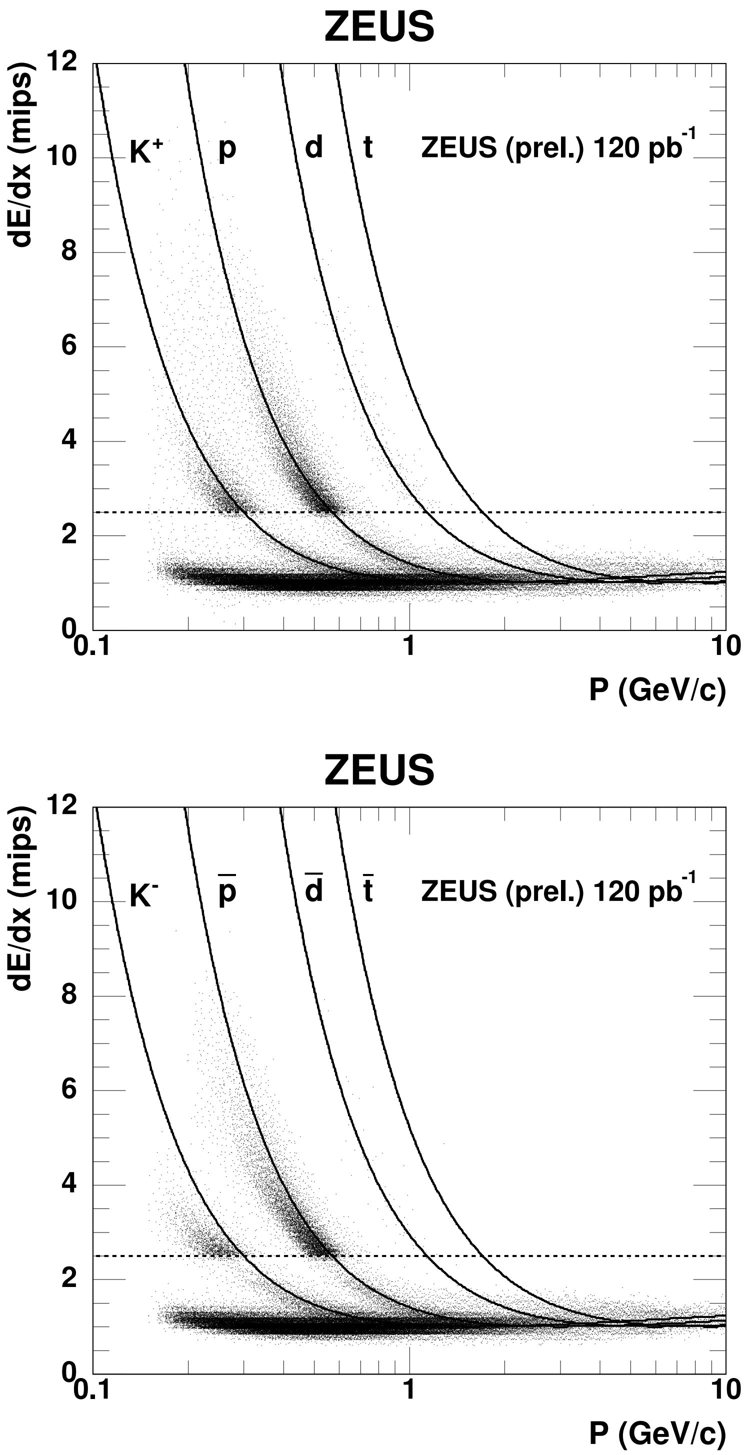

Figure 1: *The dE/dx distributions as a function of the track momentum for positive and negative tracks. The DIS events were accepted by requiring at least one track with $dE/dx > 2.5$ mips with $\Delta Z < 1\,cm$ and $DCA < 0.5\,cm$. The dE/dx is normalised to a minimum ionising particle, defined as the average truncated mean of pion tracks in the momentum range $0.3 < p < 0.4\,GeV$. The curves show the mean energy loss derived using the Bethe-Bloch equation for different particle species.*

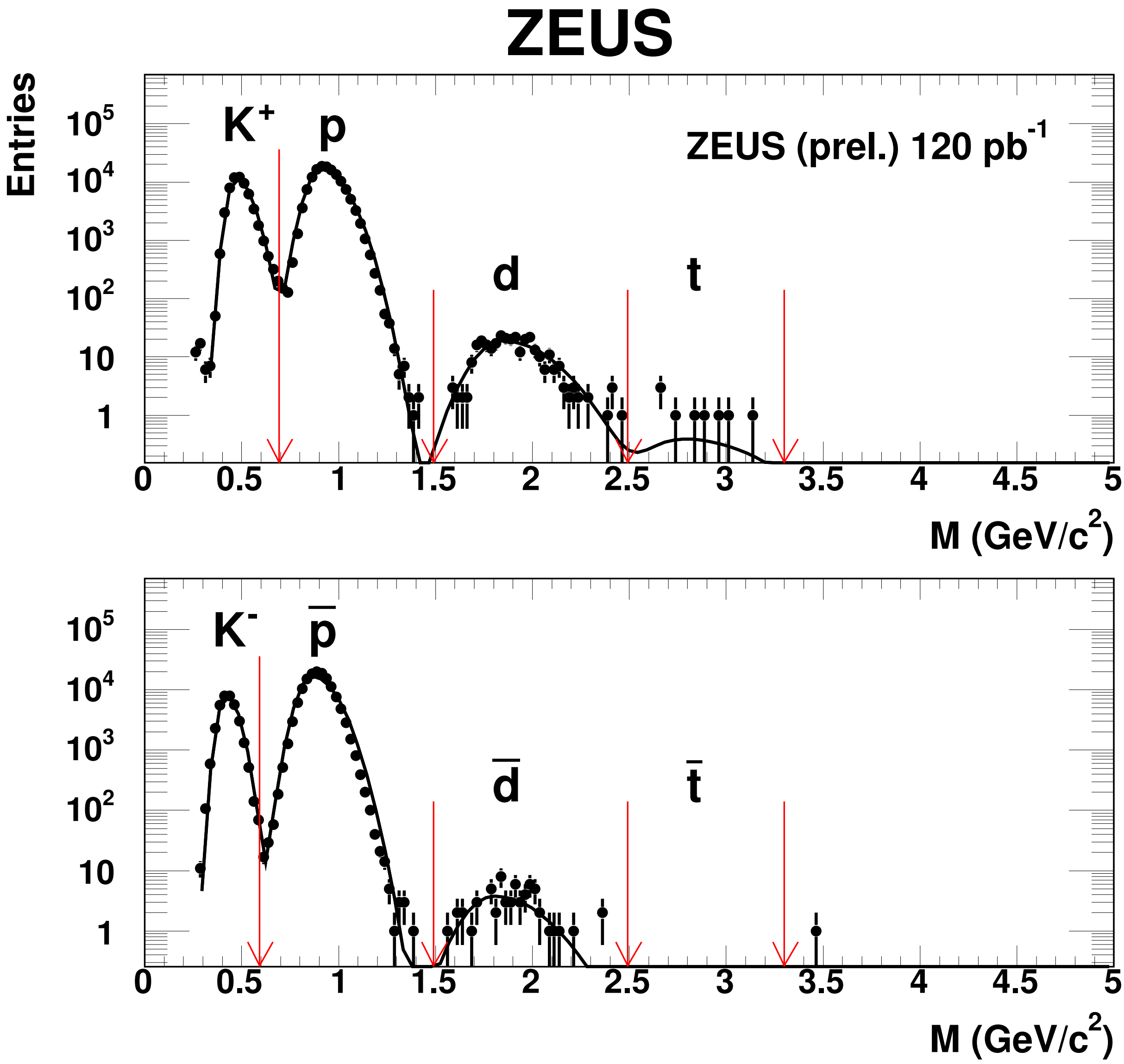

Figure 2: *The mass spectra for positive and negative particles. Tracks are selected as for Fig. 1. The mass was calculated from the track momenta and the most probable specific energy loss. The arrows show the cuts applied for the selection of proton, deuteron and triton candidates.*

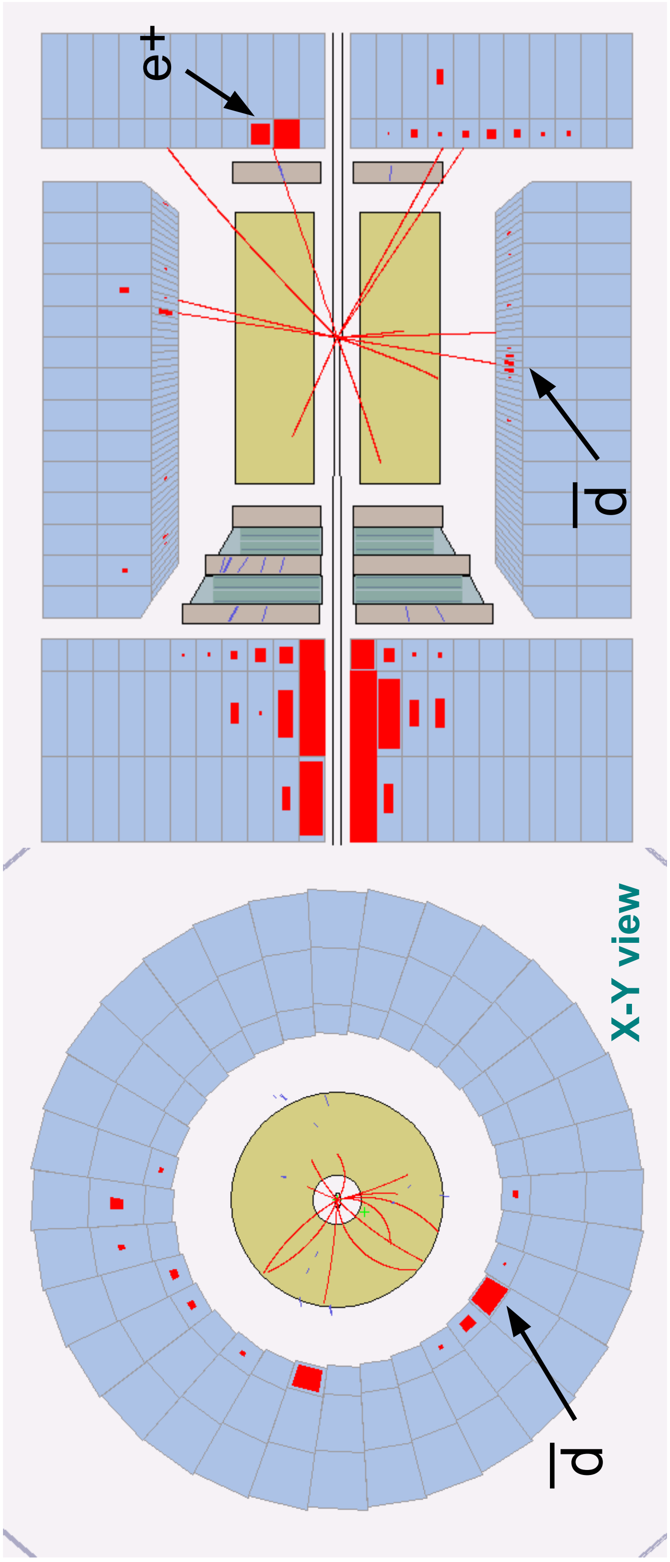

Figure 3: *A typical DIS event with one antideuteron. The event has the following characteristics:* $Q_e^2 = 45.5\ GeV^2$, $E_{e'} = 14.1\ GeV$, *12 primary-fitted tracks and* $Z_{\rm vertex} = -5.4\ cm$. *The antideuteron track, indicated by the arrow, has* $dE/dx = 2.7$ *mips and the momentum* $p = 1.1\ GeV$. *The energy deposited by this antideuteron in the calorimeter is* $3.2\ GeV$. *The antideuteron track is also characterised by* $DCA = -0.09\ cm$ *and* $\Delta Z = -0.24\ cm$ *(both variables are introduced in Sect. 5.1).*

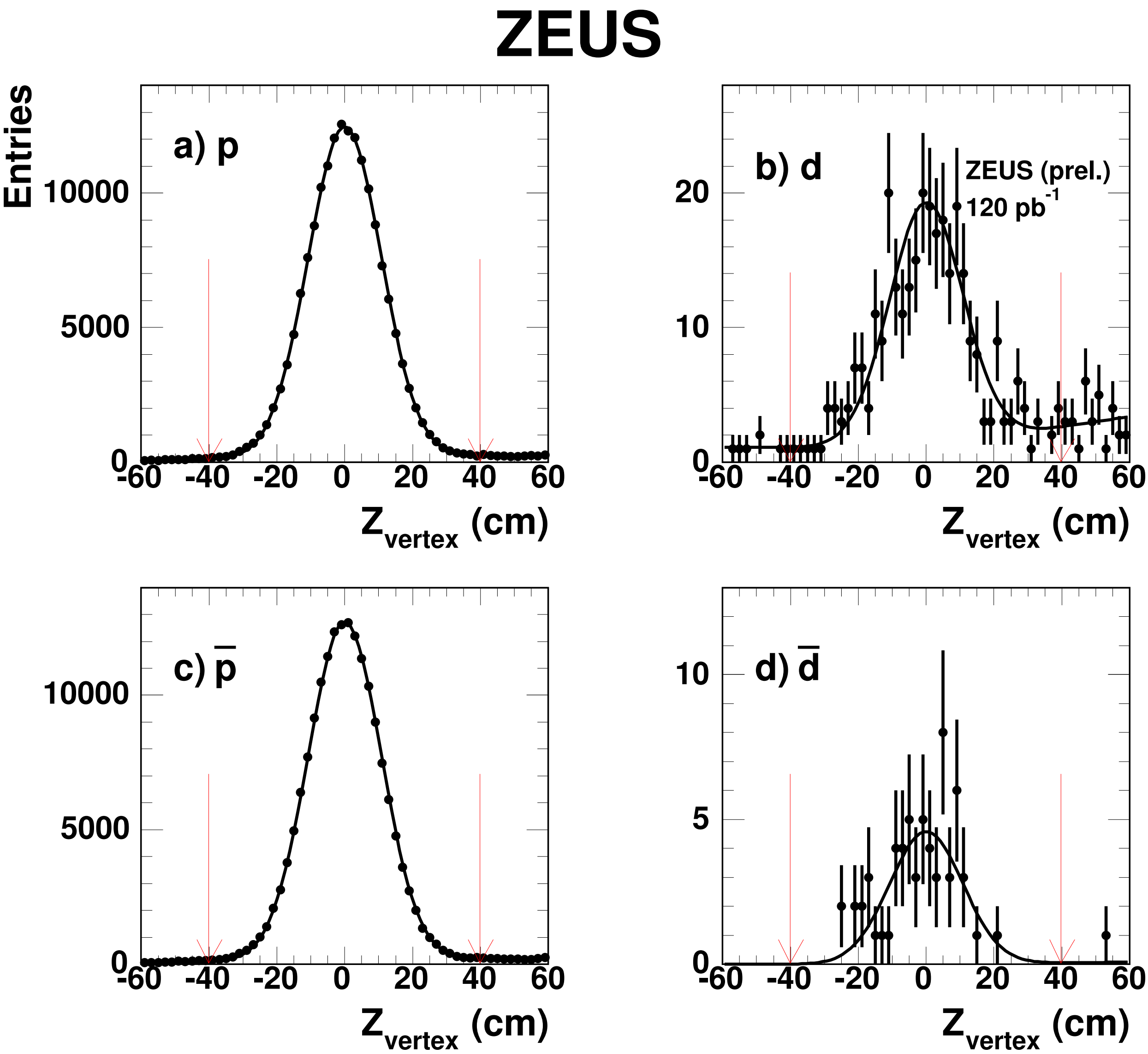

Figure 4: *The distributions of the primary vertex in z for different particle species. Particles were identified using the cuts on the mass distribution:* $0.6 < M < 1.5\,GeV$ *(for protons) and* $1.5 < M < 2.5\,GeV$ *(for deuterons). The curves show fits using a Gaussian distribution with a first-order polynomial function. The arrows show the cuts applied for the final selection.*

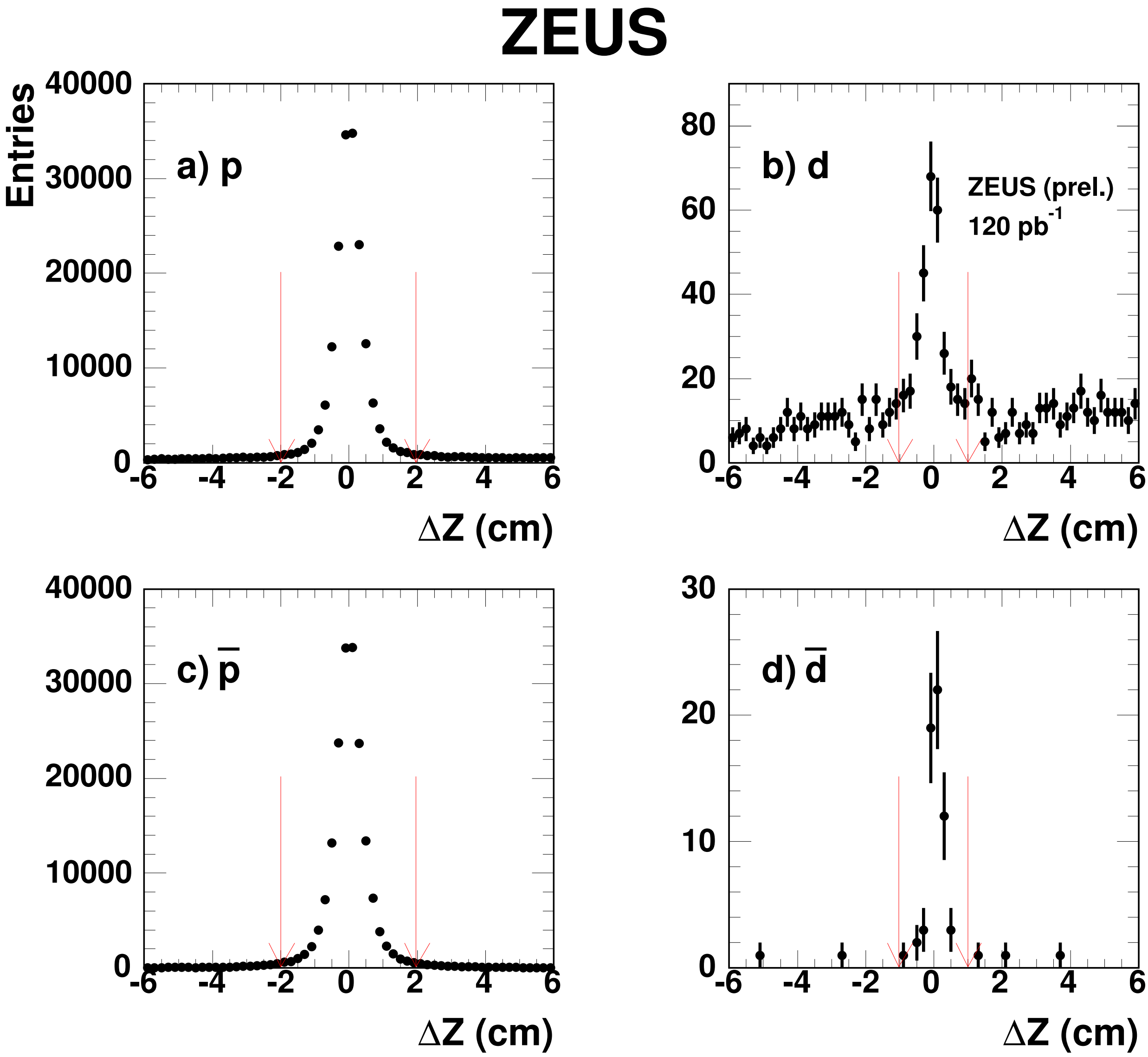

Figure 5: *The distributions of the distance of the Z-component of the track helix to the nominal interaction point with $Z_{\mathrm{vertex}} = 0$ for different particle species. The arrows show the applied cuts. Particles were selected using the mass cuts $0.6 < M < 1.5$ GeV (for protons) and $1.5 < M < 2.5$ GeV (for deuterons).*

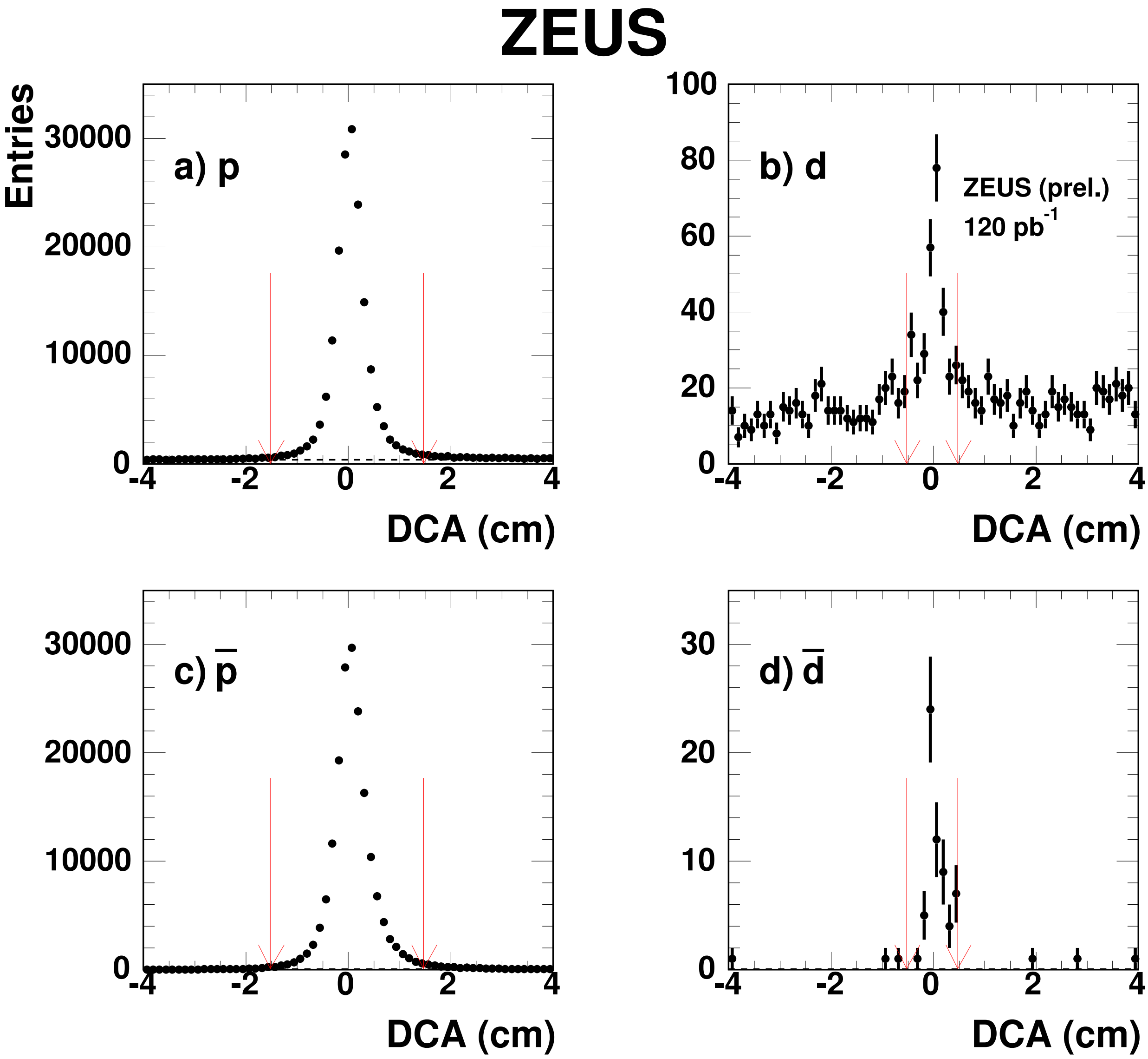

Figure 6: *The distributions of the distance of closest approach for different particle species after the cut* $| \Delta Z | < 2(1)$ *cm for protons (deuterons). Particles were identified using the cuts* $0.6 < M < 1.5$ *GeV (for protons) and* $1.5 < M < 2.5$ *GeV (for deuterons). The arrows show the signal regions for the side-band background subtraction.*

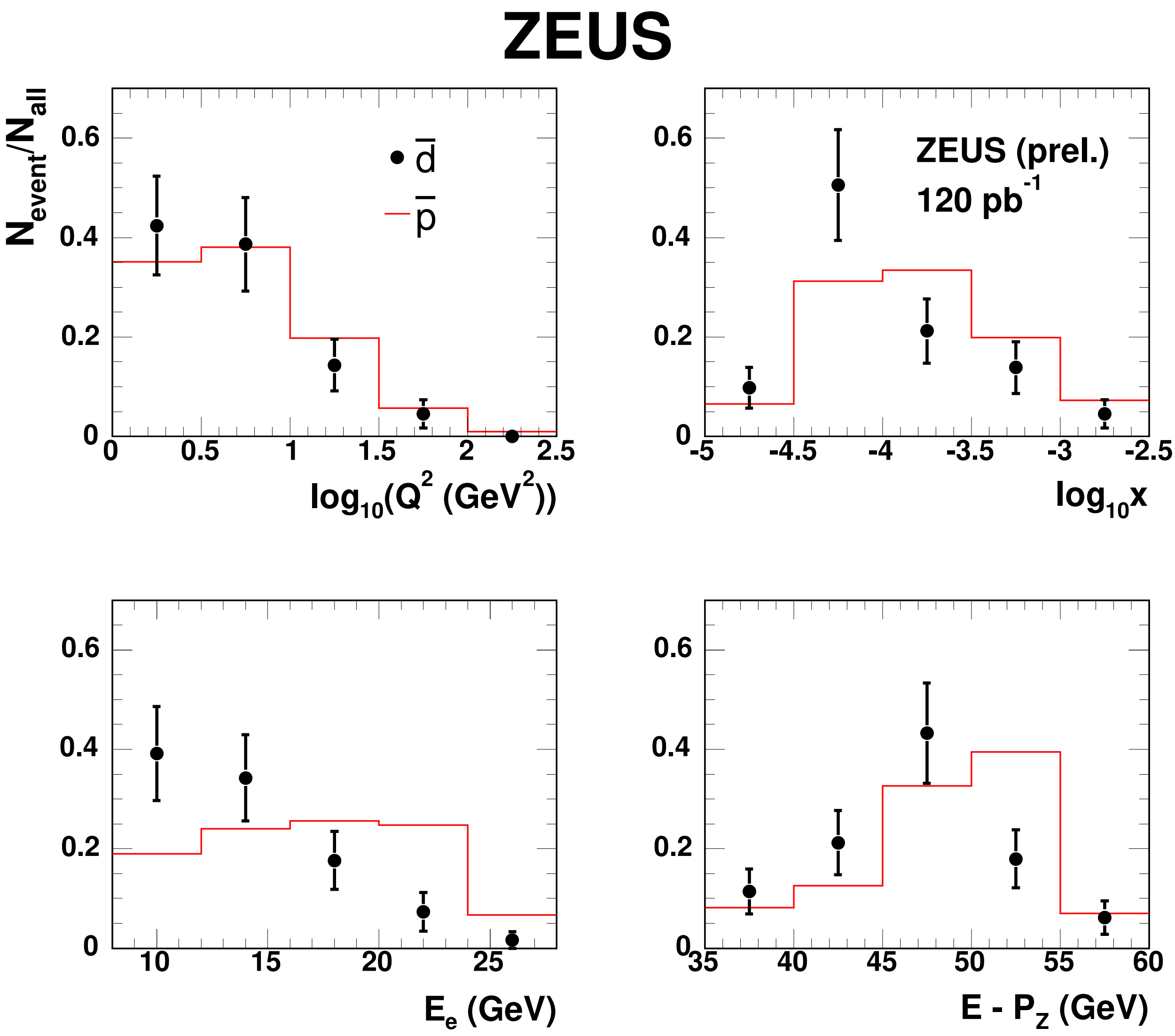

Figure 7: *The DIS distributions for events with at least one antideuteron and antiproton candidate. Particles were identified using the cuts* $0.6 < M < 1.5$ *GeV (for antiprotons) and* $1.5 < M < 2.5$ *GeV (for antideuterons)*

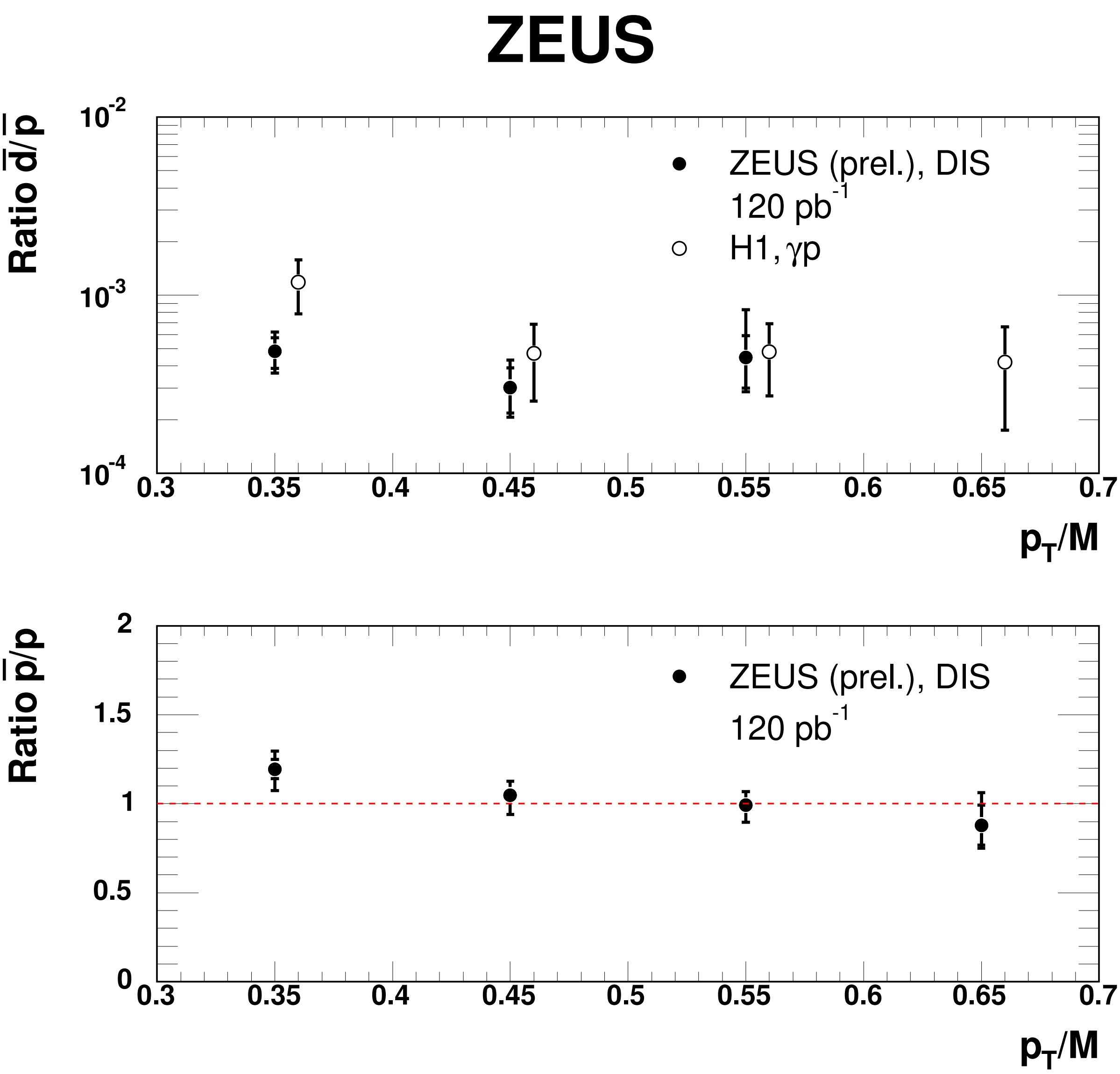

Figure 8: *The corrected $\bar{d}/\bar{p}$ production ratios compared to the H1 photoproduction results. The bottom plot shows the $\bar{p}/p$ ratio as a function of p_T/M.*